Semiconductor Physics, Quantum Electronics & Optoelectronics, 2025. V. 28, No 2. P. 183-193.

Optics

Plane-focusing Fresnel lenses for oblique incidence of light beams

E.E. Antonov[1], V.S. Lysenko[2], D.Yu. Manko[1], I.A. Martynyuk[1], V.V. Petrov[1], V.N. Zenin[1]

[1]*Institute for Information Recording, NAS of Ukraine, 2 Shpak Street, 03113 Kyiv, Ukraine*
[2]*V. Lashkaryov Institute of Semiconductor Physics, NAS of Ukraine,*
41 Nauky Avenue, 03028 Kyiv, Ukraine
Corresponding author e-mail: antv1947@gmail.com; lysenko.v@nas.gov.ua

Abstract. An algorithm for simulating parameters of microprismatic plane-focusing Fresnel lenses is proposed. An appropriate technology of manufacturing such lenses is developed. Such specialized lenses are more efficient for concentrating sunlight in photovoltaic modules of solar energetics compared to the traditional point-focusing Fresnel lenses. Plane-focusing optics is also useful for optical control systems with four-plane photodetectors for automatic moving objects tracking. This optics is typically used at normal light incidence onto photosensitive surfaces. However, lens focusing characteristics for oblique light incidence are different from the ones for normal incidence case. In this paper, the focusing characteristics of such lenses are obtained for oblique light incidence onto a registering surface. Specialized plane-focusing microprismatic lenses fabricated according to our simulation results are experimentally investigated using a collimated laser beam and computer modeling for the case of oblique light incidence.

Keywords: microprismatic plane-focusing lenses, simulating algorithm, oblique incidence of light, computer modeling.

https://doi.org/10.15407/spqeo28.02.183
PACS 07.60-j, 42.79-e, 85.60-q

Manuscript received 10.12.24; revised version received 18.04.25; accepted for publication 11.06.25; published online 26.06.25.

1. Introduction

Currently, a new kind of Fresnel transforming lenses was proposed by our author's team [1]. The main feature of such optics is the ability to form a round homogeneous light spot of a required diameter at certain focal distance in the focal plane for passed light beams. This focusing characteristic greatly differs from the one for traditional point-focusing plane Fresnel lenses, which form point image of the light source in the focal plane.

Our plane-focusing lenses are very effective in modern photovoltaic (HCPV) modules, functioning with high-concentrated sunlight [2]. Here, microprismatic Fresnel transforming lenses can totally diminish overheating of solar modules, caused by increased side currents and Ohmic losses between the HCPV cascades [3–9]. Such problem exists at non-uniform irradiation distribution at the photovoltaic surface with traditional point-focusing Fresnel optics [10–16]. The overheating process also decreases the electrical output of the module. However, all the problems related to the non-uniform irradiation of the HCPV modules can be completely resolved by applying the new transforming Fresnel lenses, which create a uniformly illuminated light circle in the lens focal plane, for concentrating sunlight [1].

The other important application of the plane-focusing optics are optical systems with four-plane photodetectors, which are used for automatic tracking of moving objects [17]. Our new transforming optics can replace a traditional pair of "diffuser–focusing lens" optical elements in such systems. At the first stage of object tracking, it is necessary to scan the space with a wide enough light beam and to evidence the very existence of such an object. For this, the light reflected from a moving object is focused by a specific lens system on a corresponding photodiode matrix to determine the direction to the object in a large enough direction-finding angle. At the next stage, plane-focusing optics [1, 2] is more convenient for accurate determining of the direction-finding characteristics of the object. This allows one to reduce the weight and dimensions of an optical module and thus increase the accuracy and reliability of moving objects monitoring.

In the examples of application of plane-focusing optics discussed above, the passing light beams were incident normally onto the lens surface. However, sometimes, light falls at the transforming surface at certain non-zero angles. The lens focusing characteristics at oblique light incidence greatly differ from those for the normal incidence case. Therefore, the main aim of our paper is to investigate the properties of the created plane-focusing Fresnel lenses for the case of oblique light incidence using a collimated laser beam and computer modeling.

2. Fabrication of plane-focusing optics

The details of the algorithm of creating plane-focusing lenses are presented in our previous papers [1, 2]. Such Fresnel lenses form a light circle of a required radius r_V with an almost homogeneous illumination distribution in the focal plane. During simulation process, the following lens parameters were used: f is the lens focal distance; D_L is the light diameter of the lens; r_V is the outer radius of the homogeneous light spot in the focal plane; r_j are the radii of the dark light zones in the focal plane, required for spot homogenization (j = 3…6); and n_0 and n_1 are the refractive indices of the medium and the material of the microprisms, respectively. The data for $n_1(\lambda)$ were taken from [18]. The following lens parameters should be obtained as a result of simulations: R_k are the radii of the lens annular prismatic zones (k = 1, 2, 3,…, N); ΔR_k is the width of each refractive k-zone of the lens; γ_k is the observation angle of the k-zone from the focus F; α_k are the prism refractive angles; and h_k is the relief depth for each k-zone, respectively.

The updated schemes of light refraction for the above lens and for a plastic matrix prototype of this lens are described in [19, 20]. Obviously, metal matrices for lens replication should have a prismatic relief reversed to the one of the lenses.

For investigating the oblique light incidence case, a set of plane-focusing lenses-originals were individually fabricated from optical polycarbonate by diamond micro-cutting according to the simulated geometrical parameters of lenses [19]. Multiple lens samples were also manufactured by thermo-pressing method [20] using special stamp-matrixes. The matrices were formed by individual diamond micro-cutting [21] of round blanks made from special aluminum alloy W-95.

A typical simulated structure of a lens relief is shown in Fig. 1 for the lens #05c2, with f = 41 mm for the wavelength λ = 1.064 μm (n_1 = 1.564), and D_L = 50 mm. This lens forms a homogeneous light spot of the radius r_V = 7.0 mm in the focal plane. It has 4 prismatic zones, as simulated according to the focusing optimization scheme FO: 04(1)-1.5(1)-3.1(1)-5.0(1) [1]. Each of the k-zones mentioned above is formed by 6, 9, 9 and 5 separate similar microprisms, respectively, the prism angle α_k and the relief depth h_k being the same. Such multiprismatic scheme is used to diminish pitch of the refractive zone ΔR_{kc} for each k-zone to the length $A_p \approx$ 1.6 mm, which is the standard one for the working cutting edge of an evaluable diamond tool [17].

A diamond instrument is used at our Institute to form the lenses-originals and the metal stamp-matrices, which are used at the next fabrication step for manufacturing multiple copies of necessary lenses from optical plastics.

2.1. Technology of diamond microcutting

The technique of diamond microcutting is now a well-established optical production technology used for formation of any lenses [22, 23]. It allows fabrication of lenses with exceptional geometrical accuracy and mirror-like surfaces. This method makes it possible to obtain high accuracy of the geometric parameters of the lens microstructure and to achieve the high cleanliness of the working refraction surfaces. For this, high performance of the diamond tool being used must be achieved. To form a cutting tool with required dimensions, it is necessary to achieve high precision of alignment of the cutting edges and to ensure precise mutual position of the edges of a cutting part of the tool. In this case, individual geometry of the cutting part of the diamond cutter is shaped based on the calculated geometric parameters of the microstructure of a circular Fresnel lens.

In the metal body of the cutter, a diamond pyramid with the cutting angle α_p is positioned in such a way that its front face BAD is inclined at an angle γ relative to the body central axis AO, so that the front face of the diamond pyramid $ABED$ is inclined at the angle γ with respect to the cutter body (Fig. 2). In view of the technological requirements, this inclination angle is

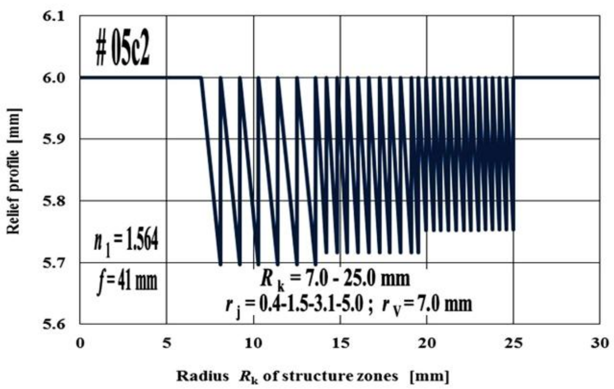

Fig. 1. Microrelief structure of the lens # 05c2 with the focus f = 41 mm, which forms a light circle with the radius r_V = 7.0 mm.

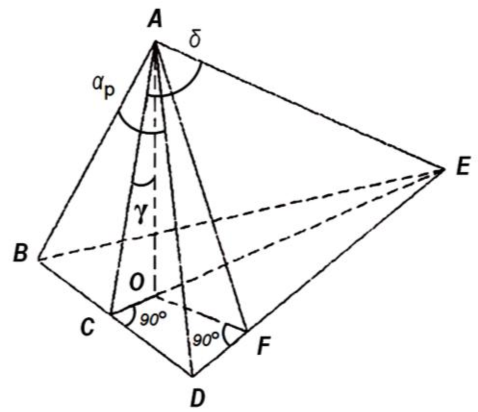

Fig. 2. Working part of a diamond cutter with the cutting angle α_p and inclination angle γ.

typically set to $\gamma = 24$ deg. If the cutter is turned around the axis AO in such a way that its front face BAD is located on the top in horizontal position, then this view will correspond to the position of the cutter on the cutting machine [19].

The requirements for the geometry of the cutting part of diamond cutter are as follows: (1) the angle of the tip of the cutter α_p should be smaller than the angle of the groove of the lens with the minimum angle $\alpha_{k\,\min}$: $\alpha_p < (90 - \alpha_{k\,\min})$; (2) the length A_p of the cutting edge of the cutter (AB or AD in Fig. 2) must be greater than the width of the working surface ΔR_k of the groove with the maximum inclined working surface: $A_p > \Delta R_k = h_k/\sin\alpha_{k\,\max}$; (3) if possible, the inclination angle of the cutting edge β_p between the face BAD and each of the faces DAE or BAE should be set to a value less than 90 degrees, but to the maximum possible one. This fact is related to the condition of tool wear resistance. The angle β_p is usually defined during manufacturing the diamond tool and is set to the value $\beta_p = 83$–84 deg., measured for the inclination angle $\gamma = 0$ deg.

To determine the angle of the tip of the cutter α_p, a groove with the minimum relief angle $(90 - \alpha_{k\,\max})$ should be selected from all the previously calculated parameters of the lens grooves, and this value is then reduced by 2-3 deg. The length of the cutting edge of the cutter A_p should be greater than the pitch of the groove with the maximum width $\Delta R_{k\,\max} = h_k/\sin\alpha_{k\,\max}$ by 0.4–0.6 mm.

Usually, a diamond crystal with the defined angle at its tip α_p and with the angle β_p at its base for $\angle\gamma = 0$ is provided. For calculating and forming the cutting edge inclination β_p^* (the angles CDE and AFO in Fig. 2), it is possible to obtain from geometrical considerations the following expression for $\angle\beta_1^*$, the inclination angle of the side face DAE to the front place BAD, for any value $\gamma \neq 0$ deg.:

$$\angle\beta_1^* = \operatorname{arctg}\left\{\left[\sin\gamma + \cos\gamma\,\operatorname{tg}(\delta-\gamma)\right]/\operatorname{tg}(\alpha_p/2)\right\}. \quad (1)$$

The value of $\angle COF$, required for positioning the tool in a special polishing machine for final treatment of the tool's side faces, is equal to $(180 - \beta_1^*)$. Hence, the inclination angle β_2^* of the side face DAF to the axis AO is

$$\angle\beta_2^* = \\ = \operatorname{arctg}\left\{\operatorname{tg}(\delta-\gamma)\cos\left[\operatorname{arctg}\left(\sin\gamma + \cos\gamma\,\operatorname{tg}(\delta-\gamma)\right)\right]/\operatorname{tg}(\alpha_p/2)\right\}, \quad (2)$$

where the angle δ between the upper face of the cutter and its rear edge is equal to $\delta = \operatorname{arctg}\left(\operatorname{tg}(\alpha_p/2)\operatorname{tg}\beta_p\right)$, where $\angle\beta_p = \angle BDE = \angle DBE$.

Specific requirements are imposed for already calculated cutter parameters. During the process of turning the lens for forming the lens relief, the rear parts of the cutter must not touch the vertical non-working surfaces of the lens relief. If this requirement is not met, the geometry of the cutter must be corrected.

Indeed, at some parameters of the microstructure of Fresnel lenses, such as radii R_k, depths h_k and inclination angles α_k of the working surfaces, as well as the parameters of the cutting part of the diamond cutter including the angle of the apex α_p and the angle of the cutting edge β_p, there is a possibility of a contact between the rear edge of the cutter and the edge of the groove formed by this cutter. To eliminate this effect, one should calculate the contact areas of the rear edge of the cutter at different values of the above-mentioned parameters of the grooves and the cutter angles. It can be obtained from geometrical considerations that the critical radius R^*_{kk}, for which the contact discussed above takes place, is equal to

$$R_{kk}^* = h_k\,\operatorname{tg}\delta/\cos(90-\alpha_k-\alpha_p/2)\times \\ \times\cos\left\{2\operatorname{arctg}\left[\operatorname{tg}\delta/\sin(90-\alpha_k-\alpha_p/2)\right]-90\right\}. \quad (3)$$

We set the real values of the cutter parameters: the angle of the cutter tip $\alpha_p = 50$ deg. and the angle of the cutting edge $\beta_p = 84$ deg. For this case, the back angle δ between the upper face of the cutter and its rear edge is equal to $\delta = \operatorname{arctg}\left(\operatorname{tg}(\alpha_p/2)\operatorname{tg}\beta_p\right) = 77.298$ deg. From (3), a series of cutter contact lines R_{kk} for different relief depths h_k depending on the angle of relief groove α_k can be easily obtained. These data for R_{kc} are presented in Table 1.

Changing the angle of the cutting edge by only one degree to $\beta_p = 83$ deg. reduces the angle of the cutter back edge δ to the value $\delta = 73.529$ deg., which significantly reduces the negative effect of touching the relief grooves by this back edge of the cutter, i.e. reduces the critical values of R_{kc}. The data similar to the ones given in Table 1 for $\delta = 77.298$ deg., but for the angle $\delta = 73.529$ deg., are given in Table 2.

The dependences calculated by expression (3) at stated above cutter parameters is shown in Fig. 3 for $\beta_p = 84$ deg. (solid lines) and $\beta_p = 83$ deg. (dotted lines).

In order to reduce the force of separating a fabricated plastic lens from the metal stamp-matrix during thermo-pressing replication process, it is necessary to

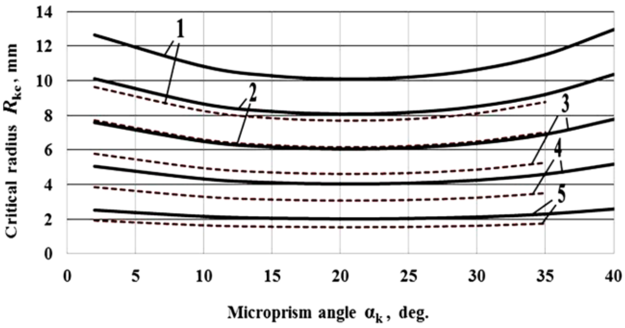

Fig. 3. Dependence of the critical radius R_{kk} on the prism angle α_k for the relief depth h_k: *1* – 0.5 mm, *2* – 0.4 mm, *3* – 0.3 mm, *4* – 0.2 mm, and *5* – 0.1 mm. Solid lines – $\beta_p = 84$ deg. dotted lines – $\beta_p = 83$ deg.

Table 1. Critical radius R_{kk} as a function of α_k for several values of h_k: α_p = 50 deg., β_p = 84 deg., δ = 77.298 deg.

h_k, mm	Microprism angle α_k, degrees							
	2	10	15	20	25	30	35	40
0.5	12.650	10.830	10.290	10.100	10.210	10.650	11.510	12.960
0.4	10.120	8.660	8.230	8.080	8.170	8.520	9.210	10.370
0.3	7.590	6.498	6.174	6.060	6.126	6.390	6.906	7.776
0.2	5.060	4.332	4.116	4.040	4.084	4.260	4.604	5.184
0.1	2.530	2.166	2.058	2.020	2.042	2.130	2.302	2.592

Table 2. Critical radius R_{kk} as a function of α_k for several values of h_k: α_p = 50 deg., β_p = 83 deg., δ = 73.529 deg.

h_k, mm	Microprism angle α_k, degrees							
	2	10	15	20	25	30	35	40
0.5	9.6436	7.7149	5.7861	3.8574	1.9287	9.6436	7.7149	5.7861
0.4	8.2582	6.6019	4.9537	3.3025	1.6512	8.2582	6.6019	4.9 37
0.3	7.8445	6.2741	4.7067	3.1378	1.5689	7.8445	6.2741	4.7067
0.2	7.6996	6.1597	4.6198	3.0799	1.5399	7.6996	6.1597	4.6198
0.1	7.7835	6.2283	4.6701	3.1134	1.5567	7.7835	6.2283	4.6701

simulate and to form lateral non-working surfaces of the microprisms in the lens and in the matrix inclined by ≈ 3 deg. [2]. For this aim, the spindle block of a 6P82 type machine, used at the Institute for Information Recording, NAS of Ukraine for forming the circular microrelief, was modernized [2] to be able to be turned by an angle ± 5 deg. in order to form relief with a reverse angle of microprisms, which is different from zero value. A general view of the modernized spindle block of the 6P82 type machine with a cutter and a cooling system during matrix manufacturing is shown in Fig. 4.

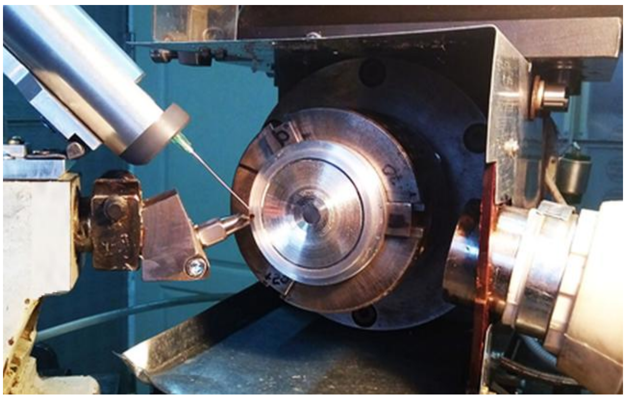

Fig. 4. General view of the spindle block of the 6P82 type machine for forming circular microrelief with a diamond cutter and a cooling system.

2.2. Method of thermo-pressing

For manufacturing polymer plane-focusing lenses, in particular from polycarbonate, a special thermo-pressing system was used. The basis of this system was a hydraulic thermo-pressing unit, which consists of a hydraulic press with heating elements. The composition of the thermo-pressing system is as follows: (1) hydraulic pressing unit; (2) heating system; (3) cooling system; and (4) control scheme for thermo-pressing system.

The hydraulic pressing unit provides the necessary force. Setting the pressure within 0.5–5.0 kg/cm^2, the total pressing force to the stamp-matrix can be set within 100–1000 kg.

The lower heating element consists of a metal housing, in which a 700 W electric heater is installed, and channels for coolant flow. The required temperature of the lower heating element is set and regulated using a 2TPM1-1 device. The maximum temperature value that can be set is 250 °C.

The lower heating element is fixed to the bed of the pneumatic press installed on adjustable metal supports, with which parallelism of the lower heating element relative to the upper one is adjusted and a thermally insulating air gap is provided.

The upper heating element consists of a housing, in which three electric heaters with a total power of 600 W are installed. It is intended for additional heating of the polymer blank of the lens and ensuring proper temperature regime of thermo-pressing.

The required temperature of the upper heating element is set and regulated using the 2TPM1-2 device, the maximum temperature value of the upper element is 200 °C.

Development of a technological mode of thermo-pressing consists in determining operating temperatures of the lower and upper heating elements and the pressure force of the hydraulic press. For polycarbonate, which is an optical structural material, the operating parameters of thermo-pressing process are experimentally determined as follows:

– pressure force of the hydraulic press of 600 kg;

– heating temperature of the upper heating element T_U = 100 °C;

– heating temperature of the lower heating element T_L = 200 °C;

– cooling temperature of the lower element T_C = 40 °C.

At such parameters, the duration of a thermo-pressing cycle is ~7.0–8.0 min.

Using thermo-pressing method, we have manufactured multiple copies of plane-focusing lenses from optical polycarbonate with metal matrixes, made from alumina alloy W-95. A general image of an appropriate matrix #05c2m, formed by diamond microcutting according to our simulation data (illustrated in Fig. 1) is shown in Fig. 5a. The lens #05c2m-#02, manufactured by thermo-pressing method with this matrix, is illustrated in Fig. 5b.

The obtained focal distribution of a passed collimated laser beam [17] for this lens for the observation distances L = 40–42 mm is shown in Fig. 6. It can be seen from this figure that the distribution is practically flat; there is a very slight dependence of the light intensity on the L-value. The width of the profiles corresponds well to our simulation data for the diameter D_V of the focal light spot, which is shown by dotted lines in Fig. 6 and corresponds to the value D_V = 14 mm. All the profiles of the focal spots were obtained with an Image J 1.53 software [24].

Hence, this lens #05c2m-#02 is one of the optimal devices for automatic control systems equipped with registering photodetectors and having a sensitive area with the diameter D_D = 14.0 mm and functioning in infrared spectral range.

(a)

(b)

Fig. 5. General view of the manufactured metal matrix #05c2m (a) and corresponding lens #05c2m-#02 (b) having the light diameter D_L = 50 mm, focal length f = 41 mm and radius r_V = 7.0 mm.

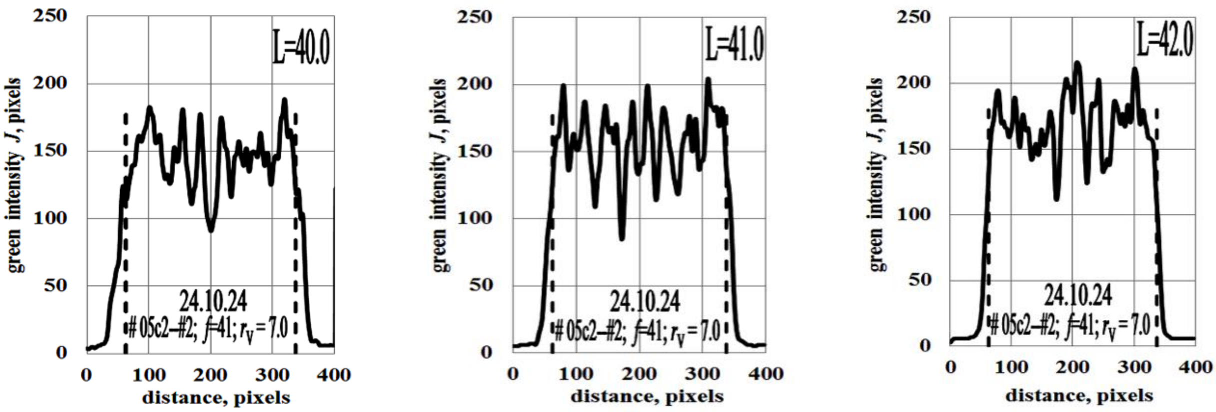

(a) (b) (c)

Fig. 6. Focal light distribution for the lens #05c2-#02 (focus f = 41 mm, radius r_V = 7.0 mm) for the observation distances L = 40 mm (a), 41 mm (b) and 42 mm (c).

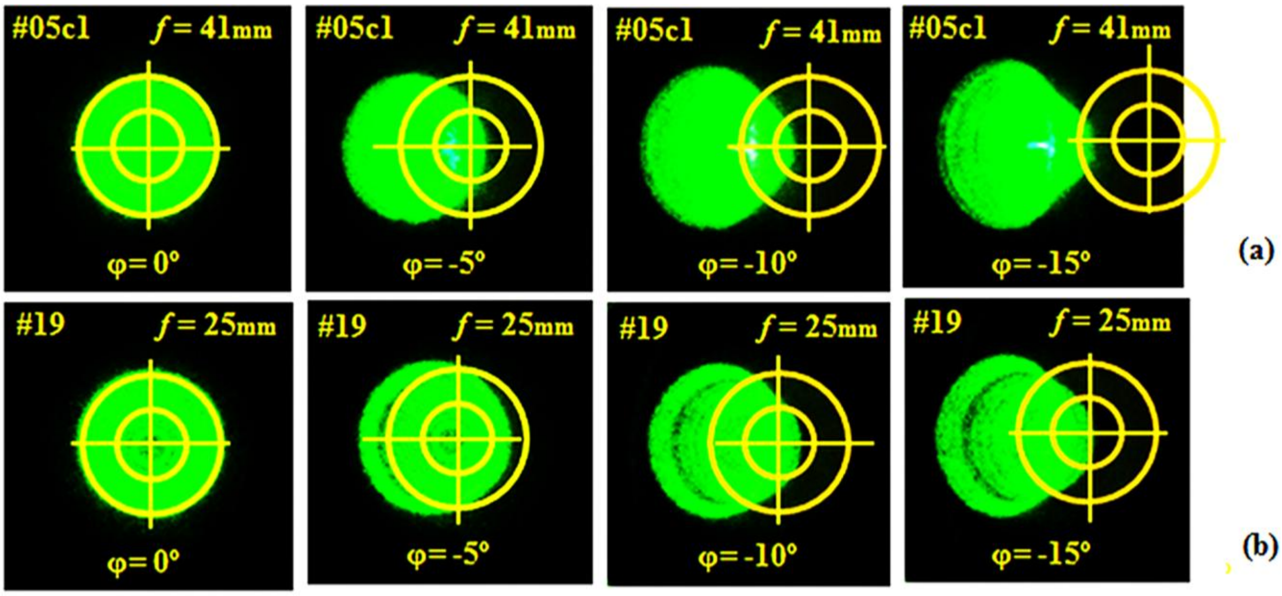

Fig. 7. Focal light spots for the lens #05c1 with the focus $f = 41$ mm and for the lens #19 with the focus $f = 25$ mm at the inclination angles φ = 0, 5, 10 and 15 deg. for nominal observation distances $L = 41$ mm (a) and $L = 25$ mm (b). The radius of the focal light spot $r_V = 4.5$ mm.

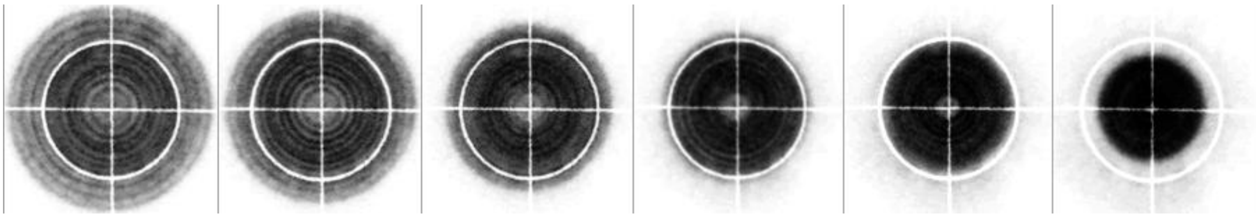

Fig. 8. Focal light spot D_V as a function of L-value for the lens #05c1: *a* – $L = 31$ mm, *b* – 33 mm, *c* – 35 mm, *d* – 37 mm, *e* – 39 mm, and *f* – 41 mm. Circles – $D_D = 14$ mm.

3. Experimental investigation of plane-focusing optics for oblique light incidence

The main feature of the transmitted light beams falling obliquely on the microprismatic structure is significant deformation of the focal light spot. Another peculiarity is the displacement of the light spot in the direction opposite to the inclination direction of the light beams. The above effect becomes more noticeable as the focal length of the lens increases. This fact is illustrated in Fig. 7, where the illumination distributions in the focal plane for the lens #05c1 having the focus $f = 41$ mm (a) and for the lens #19 with $f = 25$ mm (b), for nominal observation distances $L = 41$ mm (a) and $L = 25$ mm (b) are shown. The radii of the focal light spot for both lenses are the same and equal to $r_V = 4.5$ mm, which is shown by a larger circle in all the images.

The effect of focal spot deformation is not essential for concentrator photoelectric modules in solar energetics, since such concentrators are always equipped with a Sun tracking system to achieve the maximum efficiency of converting solar energy into electricity. However, for automatic control systems functioning with direction finding (*DF*) characteristics [17], the focal spot displacement when the lens is moving in the angular space, is very important, because this fact reduces a possible maximum tracking angle of the moving object.

To obtain the optimal *DF*-characteristics, *i.e.* the linear characteristics with the maximum bearing angle φ_{max}, it is necessary to coordinate the size of the focal light spot with the diameter D_D of the sensitive surface of a photodetector. Enlarging of the spot diameter D_V at reducing the observation distance L is illustrated in Fig. 8 for the lens-original #05c1 having the nominal spot diameter $D_V = 9.0$ mm for $L = 41$ mm. The diameter $D_D = 14$ mm is shown here by a circle. For the distance $L = 37$ mm, the diameter of the focal light spot D_V practically coincides with the diameter of the sensitive surface of photodetector D_D. This is useful for obtaining the linear *DF*-characteristics [17]. Note, that linearity is a necessary condition for adequate functioning of any automatic control system for object tracking.

When obtaining the real direction finding characteristics, the above diameter enlarging and the

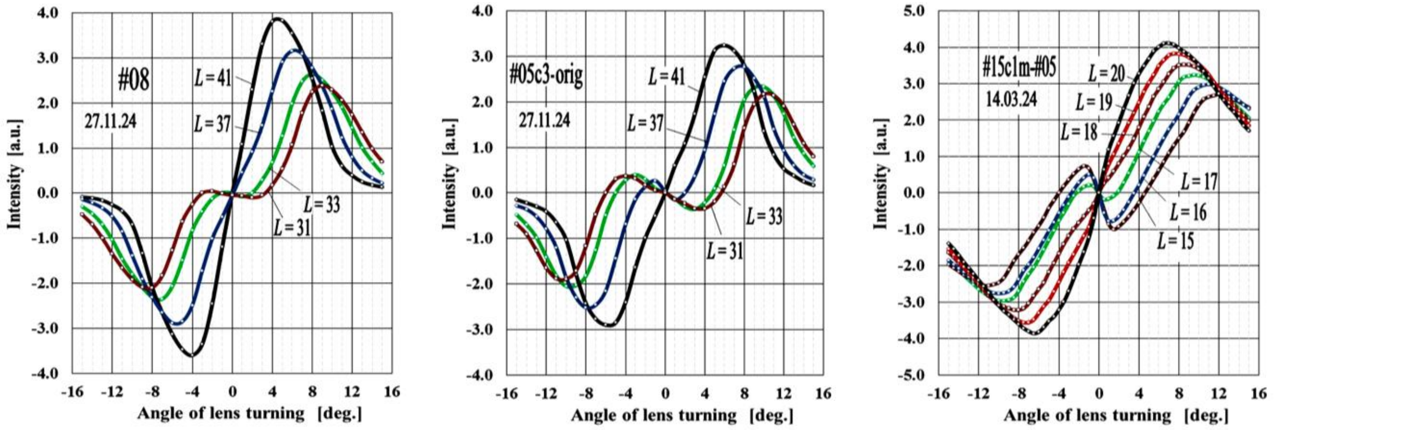

(a) (b) (c)

Fig. 9. A number of direction-finding characteristics: *a* – for the lens #08 with the focus $f = 41$ mm and $r_V = 4.5$ mm; *b* – for the lens #05c3-orig with $f = 41$ mm and $r_V = 7.0$ mm; *c* – for the lens #15c1m-#05 with $f = 20$ mm and $r_V = 4.5$ mm.

deformation of a homogeneous circular focal light spot affect the theoretical shape [17] of the *DF*-characteristics. The obtained *DF*-characteristics of the microprismatic lens #08 with the focus $f = 41$ mm and the focal light spot radius $r_V = 4.5$ mm are shown in Fig. 9a. For the nominal observation distance $L = 41$ mm, the maximum bearing angle φ_{max} is ~ 4.5 deg. for the linear "intensity-angle" zone, being just the working one. Decrease in the *L*-value increases the angle φ_{max} up to the value of ~ 8.5 deg. for $L = 33$ mm, but the *DF*-characteristics are distorted for small angles $\varphi < 4.0$ deg.

The *DF*-characteristics for the lens #05c3-orig with the same focal length $f = 41$ mm but enlarged focal spot radius $r_V = 7.0$ mm, made individually by diamond microcutting, are shown in Fig. 9b. For the nominal distance $L = 41$ mm, the maximum bearing angle is slightly enlarged to φ_{max} ~ 6.0 deg. in the linear zone. For the smaller observation distance $L = 33$ mm, the focal spot diameter D_V markedly exceeds the diameter of the used PD14M type photodetector, $D_D = 14$ mm, so that the bearing angle increases to $\varphi_{max} = 10.0$ deg. In this case, however, the *DF*-characteristics start from the negative light intensities and therefore are not suitable for proper functioning of any control system.

Note that larger as compared to $D_V = D_D = 14$ mm focal light spot for the lens #08 (Fig. 9a, curve $L = 37$) results in practically the same *DF*-characteristic with the one for the lens #05c3-orig (Fig. 9b, curve $L = 41$). It means that the main parameter shaping the *DF*-characteristic is the diameter of the light spot moving across the sensitive surface of the four-plane photodetector.

For the lens #15c1m-#05, which forms a light circle with $r_V = 4.5$ mm but has the focal length $f = 20$ mm, similar *DF*-dependences are shown in Fig. 9c. For $L = 18$ mm, the diameter of the light spot D_V coincides with the diameter of the sensitive surface of the photodetector, $D_D = 14$ mm. An almost linear characteristic is formed in the region of bearing angles up to $\varphi \approx \pm 8.5$ deg. With further decrease in the observation distance to $L = 15$–17 mm, the diameter D_V begins to exceed the value of D_D, and the *DF*-characteristics for small bearing angles $\varphi < \pm 2.0$ deg. begin to start from negative intensities. However, for $L = 15$ mm, the maximum bearing angle increases to $\varphi_{max} \approx \pm 12.0$ deg., which is useful for monitoring moving objects. Comparing data similar to those shown in Fig. 9 makes it obvious that lower focal distances *f* lead to larger maximum bearing angles φ_{max} in the linear zone of the *DF*-characteristics.

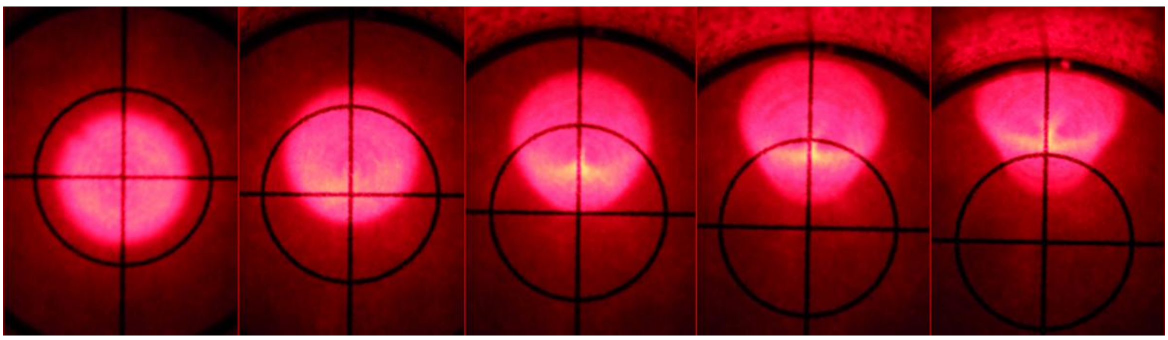

(a) (b) (c) (d) (e)

Fig. 10. Focal light spots for the lens #05c2m-#02 with $f = 41$ mm at different θ-values: *a* – θ = 00 deg., *b* – 03 deg., *c* – 06 deg., *d* – 09 deg., and *e* – 12 deg. The circles have the diameter $D_D = 16$ mm.

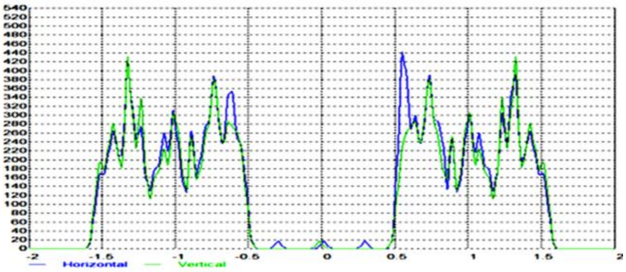

(a)

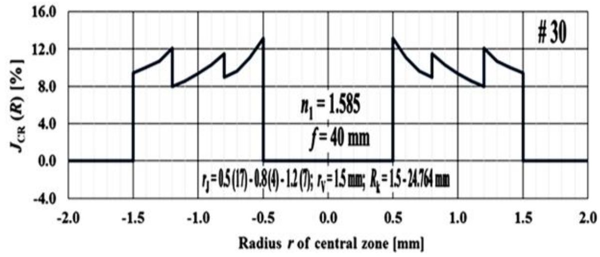

(b)

Fig. 11. Focal light spots for the lens #30 with $f = 40$ mm and $r_V = 1.5$ mm: (a) computer modeling results, (*b*) calculation data.

Our experimental results show that changes in the intensity distribution for focal light spots and spot displacement from the center as a result of the lens turning in the light beam are the main reasons for the decrease in the maximum bearing angle φ_{max}. Fig. 10 illustrates these changes for the lens #05c2m-#2 at a number of turning angles θ; a circle corresponds to the diameter $D_D = 16$ mm. The initial spot diameter $D_V = 7.0$ mm and the distance $L = 41$ mm. This lens is made by thermo-pressing method with the stamp-matrix #05c2m formed by diamond microcutting technique.

To investigate the intensity distribution in the deformed focal spots, computer modeling [25] was performed. A computer model of lenses was created by a simulation software SolidWorks-2020 [26], and beam tracing through the lens model at different incidence angles θ was carried out using TracePro [27].

As an example of beam transmission modeling, Fig. 11a illustrates a computer modulated profile of illumination distribution in the focal light spot for the lens #30, obtained from the simulated beam path through this lens. Fig. 11b shows the same profile created during the calculation of the lens parameters. Both profiles practically coincide. On the one hand, this fact indicates the high quality of the calculations of the lens geometrical parameters. On the other hand, it confirms sufficient accuracy of computer modeling for light beams passing through the lens.

The scheme of computer modeling at oblique beam incidence for the lens #05c2 is shown in Fig. 12a. A typical focal image of a passed beam through this lens for the inclination angle θ = 05 deg. in horizontal direction is shown in Fig. 12b. Red lines are the passed beams having the intensity of 66–99 %, blue lines are the reflected beams with the intensity of 0–33 %.

The obtained simulation data on focal light spot profiles for the lens #05c2 with $r_V = 7.0$ mm are shown in Fig. 13 for horizontal inclination angles θ = 0–15 deg. and nominal focus length $f = 41$ mm. For the angle θ = 0 deg., the simulation data are fully consistent with the calculated values for the light spot diameter $D_V = 14.0$ mm. The homogeneity level of the focal intensity distribution also coincides with the calculated data. However, with the increase of the angle θ, the total intensity of the passed beams is transformed into a single maximum, which moves from the center to the periphery of the image. The direction of the image movement is the opposite to the direction of lens inclination.

All the obtained factors influence the shape of the appropriate direction-finding characteristics, so that further investigations of this phenomenon are needed to increase possible maximum bearing angles φ_{max} for moving objects.

At this, the created lenses can be effectively used in solar concentration modules [2]. The computational and experimental data have confirmed that the best way to focus solar radiation beams on the sensitive surfaces of photodetector matrices is to use transforming plane-

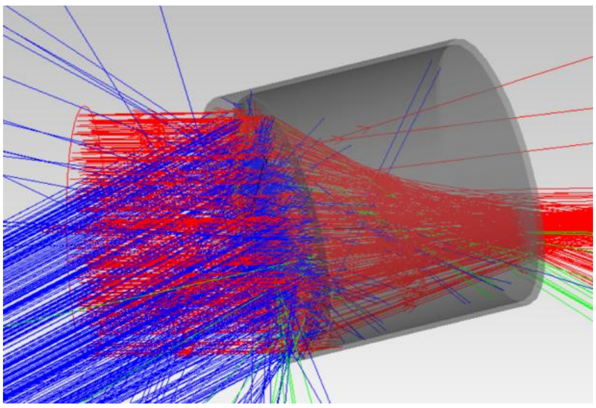
(a)

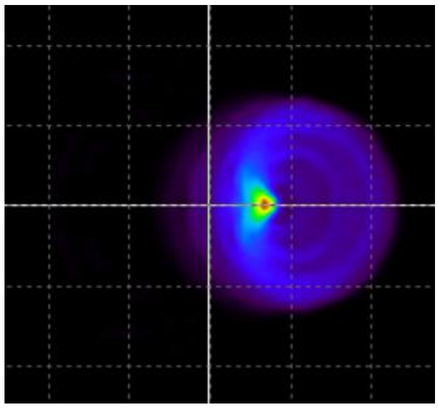
(b)

Fig. 12. Scheme of computer modeling of a beam tracing through the model #05c2 lens for the angle θ = 15 deg. (a) and image of the focal spot for horizontal inclination θ = 05 deg. (b).

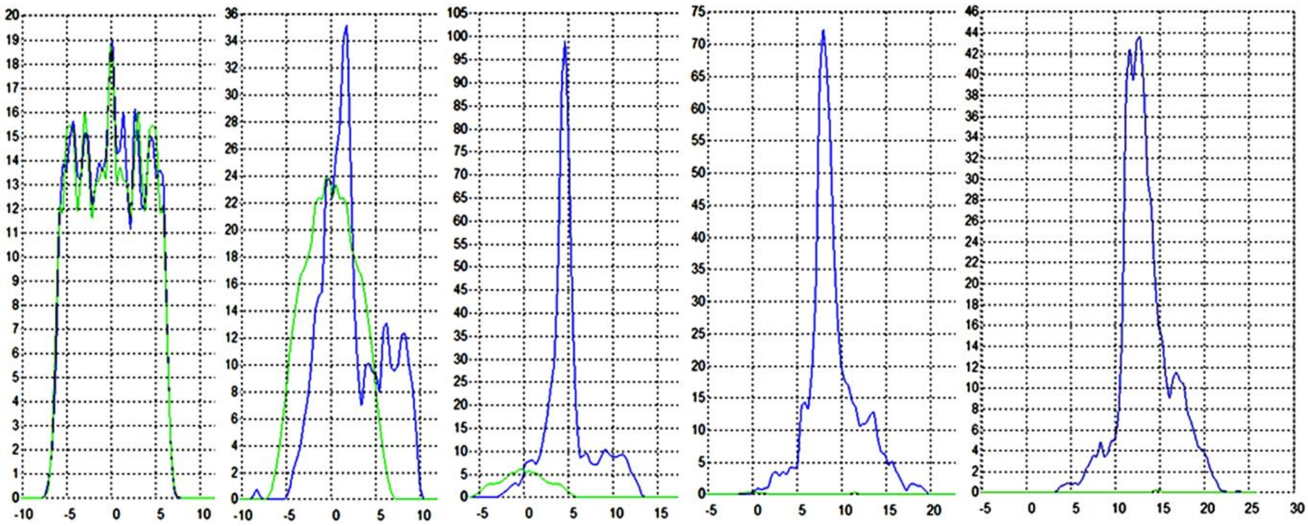

(a) (b) (c) (d) (e)

Fig. 13. Profiles of beam tracing through the model #05c2 lens for horizontal inclination angle θ = 00 deg. (a), 02 deg. (b), 05 deg. (c), 10 deg. (d), and 15 deg. (e).

focusing lenses-concentrators that create a uniformly illuminated light circle in the focal plane. Such lenses are effective for constructing solar concentration modules with minimal thermal and Ohmic losses.

4. Conclusions

A simulation algorithm for creating plane-focusing microprismatic lenses, transforming refracted light beams into a uniformly illuminated light circle in the lens focal plane, and for forming stamp-matrixes for lens replication was developed. Calculations were performed to obtain the geometrical parameters of the lenses. These parameters are adopted for lens mass manufacturing by thermo-pressing method.

According to the simulation results, the samples of specialized lens concentrators were manufactured from the optical polycarbonate by individual diamond micro-cutting technique and by thermo-pressing method with the created stamp-matrixes. The experimental study of the optical and lighting characteristics of these samples showed full compliance of the experimental data with the theoretical characteristics.

The focusing characteristics of the created lenses were investigated for the case of oblique light beam incidence onto the refractive surface of the lenses. Collimated light beams as well as computer modeling were used. The computational and experimental data confirmed that the focal light spot is markedly deformed even at small angles of inclination of beams of 5 to 10 deg. This effect enhances with increase of the lens focal length. The position of the maximum intensity of beams also moves from the center to the periphery of the image with the increase of the inclination angle in the direction opposite to the slope of the incident light beams.

For obtaining linear direction-finding characteristics of objects at the maximum bearing angle φ_{max}, the size of the focal light spot D_V should be coordinated with the diameter D_D of the sensitive surface of a used four-plane-photodetector. It is possible now to achieve the maximum value $\varphi_{max} \approx \pm 12$ deg. with evaluable plane-focusing lenses with the focus f = 15–20 mm.

The proposed specialized plane-focusing lenses-concentrators can be effectively used in solar concentration modules equipped with solar direction tracking systems, for diminishing Ohmic currents and thermal losses of photocells. The lenses for automatic control systems functioning with four-plane photodetectors should be additionally investigated for the case of oblique light incidence for specifying focusing characteristics of these lenses for the purpose of angular expansion of appropriate direction-finding characteristics of moving objects.

References

1. Fu M.L., Antonov E.E., Manko D.Yu. *et al*. Microprismatic Fresnel lens for formation of uniform light circle. *IEEE Photonics J*. 2021. **13**, No 3. P. 2200108. http://doi.org/10.1109/JPHOT.2021.3072538.
2. Fu M.L., Antonov E.E., Lysenko V.S. *et al*. Uniform illumination of concentrated sunlight in photovoltaic solar modules with plane-focusing Fresnel lenses. *IEEE Photonics J*. 2023. **15**, No 4. P. 5008080. http://doi.org/10.1109/JPHOT.2023.3288155.
3. Benitez P., Minano J.C., Zamora P. *et al*. High performance Fresnel-based photovoltaic concentrator. *Opt. Express*. 2010. **18**(S1). P. A25–A40. http://doi.org/10.1364/OE.18.000A25.
4. Sornek K., Filipowicz M., Jasek J. The use of Fresnel lenses to improve the efficiency of photovoltaic modules for building-integrated concentrating photovoltaic systems. *J. Sustain. Dev.*

Energy, Water Environ. Syst. 2018. **6**, No 3. P. 415–426. http://doi.org/10.13044/j.sdewes.d6.0204.

5. Sahin F.E., Yılmaz M. High concentration photovoltaics (HCPV) with diffractive secondary optical elements. *Photonics*. 2019. **6**. P. 68. http://doi.org/10.3390/photonics6020068.
6. Xie W.T., Dai Y.I., Wang R.Z., Sumathy K. Concentrated solar energy applications using Fresnel lenses: A review. *Renew. Sust. Energ. Rev*. 2011. **15**. P. 2588–2606. http://doi.org/10.1016/j.rser.2011.03.031.
7. Baig H., Heasman K.C., Mallick T.K. Nonuniform illumination in concentrating solar cells. *Renew. Sust. Energ. Rev*. 2012. 16. P. 5890–5909. http://doi.org/10.1016/j.rser.2012.06.020.
8. Kiyaee S., Saboohi Ya., Moshfegh A.Z. A new designed linear Fresnel lens solar concentrator based on spectral splitting for passive cooling of solar cells. *Energy Conv. Manag*. 2021. **230**. P. 113782. http://doi.org/10.1016/j.enconman.2020.113782.
9. Zhang Z., Yan J., Kuriyagawa T. Manufacturing technologies toward extreme precision. *Int. J. Exteme Manuf*. 2019. **1**. P. 022001. http://doi.org/10.1088/2631-7990/ab1ff1.
10. Yamada N., Okamoto K. Experimental measurements of a prototype high concentration Fresnel lens CPV module for the harvesting of diffuse solar radiation. *Opt. Express.* 2014. **22**, No 101. P. A28–A34. http://doi.org/10.1364/OE.22.000A28.
11. Zhang J.J., Qu Z.G., Zhang J.F. Diode model of nonuniform irradiation treatment to predict multiscale solar-electrical conversion for the concentrating plasmonic photovoltaic system. *Appl. Energy*. 2022. **324**. P. 119698. https://doi.org/10.1016/j.apenergy.2022.119698.
12. Bachhav C.Y., Sonawwanay P.D. Study on design and performance enhancement of Fresnel lens solar concentrator. *Mater. Today: Proc*. 2022. **56**, No 5. P. 2873–2879. http://doi.org/10.1016/j.matpr.2021.10.168.
13. Hayashi N., Inoue D., Matsumoto M. *et al*. High-efficiency thin and compact concentrator photovoltaics with micro-solar cells directly attached to a lens array. *Opt. Express*. 2015. **23**, No 11. P. A594–A602. http://doi.org/10.1364/OE.23.00A594.
14. Beltagy H. A secondary reflector geometry optimization of a Fresnel type solar concentrator. *Energy Conv. Manag*. 2023. **284**. P. 116974. http://doi.org/10.1016/j.encnman.2023.116974.
15. Montanet E., Rodat S., Falcoz Q., Roget F. Influence of topography on the optical performances of a Fresnel linear asymmetrical concentrator array: The case of the ELLO solar power plant. *Energy*. 2023. **274**. P. 127310. http://doi.org/10.1016/j.energy.2023.127310.
16. Ju X., Pan X., Zhang Z. *et al*. Thermal and electrical performance of the dense-array concentrating photovoltaic (DA-CPV) system under nonuniform illumination. *Appl Energy*. 2019. **250**. P. 904–915. http://doi.org/10.1016/j.apenergy.2019.05.083.
17. Antonov E.E., Lapchuk A.S., Petrov V.V. *et al*. Photodetector module of optoelectronic control systems for tracking the moving objects. *SPQEO*. 2022. **25**. P. 315–322. http://doi.org/10.15407/spqeo25.03.315.
18. Sultanova N., Kasarova S. and Nikolov I. Dispersion properties of optical polymers. *Acta Phys. Pol. A*. 2009. **116**. P. 585–587. http://doi.org/10.12693/APhysPolA.116.585**.**
19. Petrov V., Kryuchyn A., Antonov E. *et al*. Optical Phenomena in Microprism Diagnostic Set KK-42. *Proc. SPIE*. 2011. **8011**. P. 80119A. 22 General Congress on Optics “ICO-22”, 15–19 August, 2011, Puebla, Mexico. http://doi.org/10.1117/12.900751.
20. Fu M.L., Antonov E., Manko D. *et al*. Achromatic refractive-diffractive double-relief microprisms. *Opt. Laser Eng*. 2020. **126**. P. 105903. http://doi.org/10.1016/j.optlaseng.2019.105903.
21. Brinksmeier E., Glabe R., Schonemann L. Diamond micro chiseling of large-scale retroreflective arrays. *Precis. Eng*. 2012. **36**. P. 650–657. http://doi.org/10.1016/j.precisioneng.2012.06.001.
22. Tan N.Y.J., Lim Z.H., Zhou G. *et al*. Design and fabrication of composite polygonal Fresnel lenses. *Opt. Express*. 2021. **29**, No 22. P. 36516–36534. http://doi.org/10.1364/OE.436290.
23. Tan N.Y.J., Neo D.W.K., Zhang X. *et al*. Ultra-precision direct diamond shaping of functional micro features. *J. Manuf. Process*. 2021. **64**. P. 209–223. http://doi.org/10.1016/j.jmapro.2020.12.064.
24. Jmage J Program. http://soft.mydiv.net/win/download-ImageJ.html.
25. Ahmadpour A., Dejamkhooy A., Shayeghi H. Optimization and modelling of linear Fresnel reflector solar concentrator using various methods based on Monte Carlo ray-trace. *Solar Energy*. 2022. **245**. P. 67–79. http://doi.org/10.1016/j.solener.2022.09.006.
26. Shen H., Wang G. A tetrahedron-based inhomogeneous Monte Carlo optical simulator. *Phys. Med. Biol*. 2010. **55**, No 4. P. 947–962. http://doi.org/10.1088/0031-9155/55/4/003.
27. Campeau N., Wei A., Gajjar A. *et al*. Assessing tissue interrogation volume of an implantable optical sensor using TraceRro ray tracing software. *Multiscale Imaging and Spectroscopy*. 2024. P. 12827. http://doi.org/10.1117/12.3003431.

Authors’ contributions

Antonov E.E.: conceptualization, formal analysis, investigation, validation, visualization, writing – original draft.

Lysenko V.S.: conceptualization, methodology, formal analysis, supervision, writing – review & editing.

Manko D.Yu.: investigation, validation, visualization, writing – review & editing.

Martynyuk I.A.: investigation, validation, software and hardware.

Petrov V.V.: investigation, project administration, supervision, writing – review & editing.

Zenin V.N.: investigation, validation, software and hardware.

Authors and CV

Eugene Antonov graduated from the Moscow Physical-Engineering Institute with the M.S. Degree in Experimental Physics. He obtained a PhD degree in Optics and Optical Diagnostics (1978). Doctor of Engineering Sciences in Microprism Simulation (2020). He is the Leading Researcher at the Institute for Information Recording, NASU. Now he specializes in optical properties of microprisms. Authored more than 140 scientific works, including 2 monographs and 13 patents. http://orcid/0000-0003-4471-8287

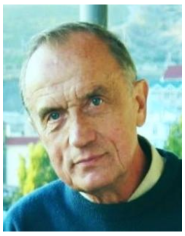

Volodumyr Lysenko, Doctor of Sciences in Physics of Semiconductors and Dielectrics, Corresponding Member of the NAS of Ukraine, Chief Researcher at the V. Lashkaryov Institute of Semiconductors Physics, NASU. His research areas are micro-, nano-, opto-electronics, information technologies, and nanoparticles for antiviral and anticancer therapy. Authored 5 monographs and more than 350 scientific works, 216 of which are included in the Scopus databases. http://orcid.org/0000-0001-9948-9499

Dmytro Manko has obtained his PhD degree (2011) in the field of optical properties of metals. His research interests are computer science, applied optics, and light polarization. Authored more than 70 scientific works, 27 of which are indexes by the Scopus databases, 3 monographs and more than 10 patents. E-mail: dmitriy.manko@gmail.com, http://orcid.org/0000-0003-1848-2952

Ivan Martynyuk graduated from the Kiev Polytechnic Institute in 1972. He is a specialist in electro-technical field, working at state energy enterprises for many years. Now he conducts precise experiments in pneumatic pressing and hydraulics thermo-pressing technology, and constructs appropriate control and measuring instruments for manufacturing final microprismatic products from optical plastics.

Viacheslav Petrov, Doctor of Sciences, Professor, Academician of the NAS of Ukraine, Director of the Institute for Information Recording, NAS of Ukraine. Authored over 700 publications, 230 patents, and 15 books. Received 16 Ukrainian and international awards. The area of his scientific interests includes information technologies, laser recording, and nanotechnologies.
E-mail: petrov@ipri.kiev.ua,
http://orcid.org/0000-0002-7265-9889

Vladimir Zenin graduated from the National Technical University of Ukraine "Igor Sikorsky Kyiv Polytechnic Institute". He is a Researcher at the Institute for Information Recording, NASU. He has carried out a series of design and research works on the development of technological equipment for implementation of diamond microcutting method, investigated optical properties of retroreflective devices and homogenizers for optical radiation. Authored of more than 40 scientific works and patents.
E-mail: zen51vlad@gmail.com,
http://orcid.org/0009-0005-1663-9743

Плоско-фокусувальні Френелівські лінзи при нахиленому падінні світлових променів

Е.Е. Антонов, В.С. Лисенко, Д.Ю. Манько, І.О. Мартинюк, В.В. Петров, В.Н. Зенін

Анотація. Запропоновано алгоритм моделювання параметрів мікропризмових плоско-фокусувальних лінз Френеля. Розроблено відповідну технологію їх виготовлення. Такі спеціалізовані лінзи є більш ефективними у фотоелектричних модулях сонячної енергетики для концентрації світла у порівнянні з традиційними точковими лінзами Френеля. Плоско-фокусувальна оптика корисна також в оптичних системах управління з чотириплощинними фотодетекторами для автоматичного відстеження рухомих об’єктів. Зазначена оптика зазвичай використовується при нормальному падінні світла на світлочутливі поверхні. Однак фокусувальні характеристики лінз для випадку похилого падіння світла відрізняються від характеристик для нормального падіння. У роботі отримано фокусувальні характеристики плоско-фокусувальних лінз для похилого падіння світла на реєструючу поверхню. Спеціалізовані плоско-фокусувальні мікропризмові лінзи, виготовлені за результатами нашого моделювання, експериментально досліджено за допомогою колімованого лазерного випромінювання та методами комп’ютерного моделювання для випадку похилого падіння світла.

Ключові слова: мікропризматичні плоско-фокусувальні лінзи, алгоритм моделювання, похиле падіння світла, комп’ютерне моделювання.